03,07

Formation of quasi-two-dimensional layers of bismuth nanoparticles in epitaxial layers of gallium arsenide

© E.D. Polenok[1,2], N.A. Bert[1], A.A. Ivanov[1], L.A. Snigirev[1], V.I. Ushanov[1], V.V. Preobrazhenskii[3], M.A. Putyato[3], B.R. Semyagin[3], M.A. Yagovkina[1], V.V. Chaldyshev[1,¶]

[1] Ioffe Institute,
St. Petersburg, Russia
[2] Peter the Great Saint-Petersburg Polytechnic University,
St. Petersburg, Russia
[3] Rzhanov Institute of Semiconductor Physics, Siberian Branch, Russian Academy of Sciences,
Novosibirsk, Russia

¶ E-mail: chald.gvg@mail.ioffe.ru

Received July 8, 2024
Revised July 9, 2024
Accepted July 10, 2024

By delta-doping gallium arsenide layers with bismuth during low-temperature molecular beam epitaxy (MBE) followed by annealing, quasi-two-dimensional layers of bismuth nanoparticles were obtained in a matrix of epitaxial gallium arsenide. The low epitaxy temperature ensures the formation of a high concentration of nonstoichiometric defects in the material, primarily antisite defects [As_{Ga}] and gallium vacancies. The migration of these defects during annealing leads to the formation of both small precipitates in the LT-GaAs layers and larger nanoinclusions enriched with bismuth, located on the Bi delta layers.

Keywords: non-stoichiometric GaAsBi, molecular-beam epitaxy, precipitation, X-ray diffractometry, transmission electron microscopy, optical absorption.

DOI: 10.61011/PSS.2024.09.59214.183

1. Introduction

One of the important directions on modern optoelectronics is implementation of localized surface plasmon resonance (LSPR). Reason of increased interest is that using LSPR it is possible to improve by several times the interaction between light and substance, which is in high demand in various applied areas [1]. Last achievement relating LSPR are described in recently published review articles [2–6]. For example, based on plasmon nanoparticles we can create biodetectors with extremely low sensitivity limit [6,7]. Systems of plasmon nanoparticles, integrated into semiconductor materials, are able to increase the efficiency of solar panels [8,9], significantly change optical properties of structures [10–12], increase by several times the Raman scattering [13–15], and provide possibility of ultrafast processing of qubits in a quantum computer [16].

The problem of LSPR implementation in semiconductor environment occurs. As example for consideration we take gallium arsenide as semiconductor most studied and used in optoelectronics. Effective formation of metal nanoparticles in matrix of gallium arsenide is currently possible only from some elements of fifth group, this significantly minimizes the set of suitable materials and removes from consideration the most popular in plasmonics metals, such as silver, gold, platinum etc [1]. Technologically it is possible to form nanoparticles of gold or silver on surface of the semiconductor [16], but their formation inside the bulk of epitaxial layer of semiconductor structure currently is practically impossible task. Another problem is that GaAs is not transparent in optical range for photons with energy exceeding the band gap of this semiconductor (1.4 eV at room temperature). So, even if LSPR is implemented in matrix of gallium arsenide using metal nanoparticles, it can stay beyond the transparency window of the semiconductor matrix.

Of all the materials that were ever successfully embedded in the gallium arsenide matrix as nanoinclusions, bismuth implements LSPR that is closest to the transparency window of GaAs [17]. In addition, the plasmon resonance peak is by its nature quite broad and partially extends beyond the edge of GaAs transparency window, which is why it can be visible in optical measurements, especially if it is enhanced, for example, using Bragg resonance [18]. Thus, formation of bismuth nanoparticles in gallium arsenide matrix, in particular, by delta-doping, is very important task in modern plasmonics.

The effective growth of semiconductor structures containing bismuth can be performed using method of molecular-beam epitaxy (MBE). But under conditions optimal for the growth of gallium arsenide the bismuth is very poorly embedded into the lattice, so growth of such structures shall be performed in non-equilibrium conditions at low temperature (LT) 150−200°C. If the molecular flow of arsenic significantly exceeds the flow of gallium, then a large number of corresponding antisite defects and gallium vacancies will form in the growing epitaxial LT-GaAs

film [19]. For nanoparticles formation in such material, it shall be subjected to additional heat treatment. During the annealing process the point defects associated with non-stoichiometric growth conditions start migration, this results in formation of nanoparticles comprising elements of fifth group [20]. In case of low-temperature $GaAs_{1-x}Bi_x$ ($x \approx 0.02$) nanoparticles comprise almost pure bismuth [21–23], have rhombohedral atomic structure and almost spherical shape with diameter of 10–20 nm.

In present paper the formation of nanoparticles in GaAs layers, grown by molecular-beam epitaxy at low temperature and delta-doped with Bi is studied. Process of formation of nanoparticles of fifth group in such material will be considered, as well as some of its optical properties, excluding features of optical interaction of plasmon nanoparticles with light.

2. Specimens and experimental methods

2.1. Samples

The studied sample was grown using the MBE method on a semi-insulating GaAs substrate with orientation $(001) \pm 0.5°$. The processes were controlled on the growth surface using a reflected high-energy electron diffraction (RHEED) method. Density of molecular flows As_4 and Bi was measured using a manometer sensor of ionization vacuum gauge that was inserted in the growth region for the measurement period. The growth rate was determined by oscillations of mirror reflex of RHEED pattern. The substrate temperature was measured using readings of calibrated thermocouple attached to the manipulator heater. The thermocouple was calibrated according to the transition temperatures of gallium arsenide surface structures.

After protective oxide layer removal a buffer GaAs layer 0.3 μm thick was grown on the substrate surface, with growth rate 1 μm/h. The growth was performed at temperature 580°C under the conditions of superposition of surface superstructures $((2)(3) \times (4)(6))$. This provided growth conditions similar to stoichiometric conditions.

Upon growth completion of the buffer layer the substrate was cooled to 200°C and superlattice (SL) comprising 24 periods was grown. The period comprised layers of LT-GaAs 140 nm thick and delta-layers of Bi with thickness of one monolayer (ML). The growth rate was 1 μm/h. Pressure in flow of arsenic and bismuth in the growth zone was, respectively, $P_{As4} = 3 \cdot 10^{-5}$ Torr and $P_{Bi} = 8 \cdot 10^{-8}$ Torr. After growth of LT-GaAs layer flows of gallium and arsenic overlapped, gate of Bi source opened, and bismuth layer 1 ML thick was deposited. Deposition time was calculated by using change of intensity of mirror reflex of RHEED. Then flow was stopped and flows of arsenic and gallium were supplied.

At initial stage of GaAs layers growth in RHEED pattern a mesh of cords of main reflexes, which leads to the conclusion about the atomic surface smoothness and high crystalline perfection. Gradually in RHEED pattern the diffusion scattering occurs, it increases with increase in thickness of growing layer. This phenomenon may be due to internal stresses increasing in growing heterostructure, caused by both capturing of excess arsenic, and effect of Bi delta-layers. To prevent relief development of growing structure, after each fifth LT-GaAs layer the growth was stopped, and structure was heated to 500°C. Then structure was cooled to temperature 200°C, and growth started by 1 ML Bi deposition. Such intermediate annealing resulted in surface smoothening, which was observed via change in RHEED pattern. The intermediate annealing of the structure was carried out four times. The upper four periods of the structure were not annealed.

The grown sample was split into four parts after growth. One part was not subjected to any treatments (as grown), three other parts were annealed for 15 min at temperatures 400, 500 and 600°C. Annealing was performed in growth chamber of the MBE unit under overpressure As_4.

2.2. X-ray diffractometry

For structural characterization of samples a high-resolution X-ray diffraction (HRXRD) was used. Diffraction reflection curves (DRC) were obtained in diffractometer D8Discover (Bruker AXS (Germany)) equipped by source with rotating anode (cathode current — 100 mA, accelerating voltage 45 kV) and PSD (position sensitive detector) Lynxeye. The diffraction curves were obtained in double-crystal geometry using 4x slit monochromator Ge (022).

2.3. Transmission electron microscopy

To study nanostructure of system of nanoinclusions in the sample the transmission electron microscope (TEM) was used. Samples were prepared in cross section (110) according to standard procedure comprising preliminary mechanical thinning and ion sputtering. Measurements were performed using the electronic microscope JEM-2100F (JEOL, Tokyo, Japan) with accelerating voltage 200 kV, equipped with energy-dispersive X-ray spectrometer (EDXS) Quantax 400 STEMXFlash 6T 30 (BrukerAXS, Karlsruhe, Germany).

2.4. Optical spectroscopy

The experimental study of the optical properties of the obtained samples in the visible and infrared spectral regions at room temperature (300 K) was carried out using optical reflection and transmission spectroscopy. Optical reflection and transmission spectra were measured in geometry of normal incidence in wavelength range 600–1500 nm. LS-1 (OceanOptics) source was utilized to generate the probing radiation. Optical fiber cables were used to transmit light between components of experimental unit. The spectra were registered using spectrometers Ocean Optics NIRQuest-512 and QE65000. Spectra were processed using software SpectraSuite from Ocean Optics.

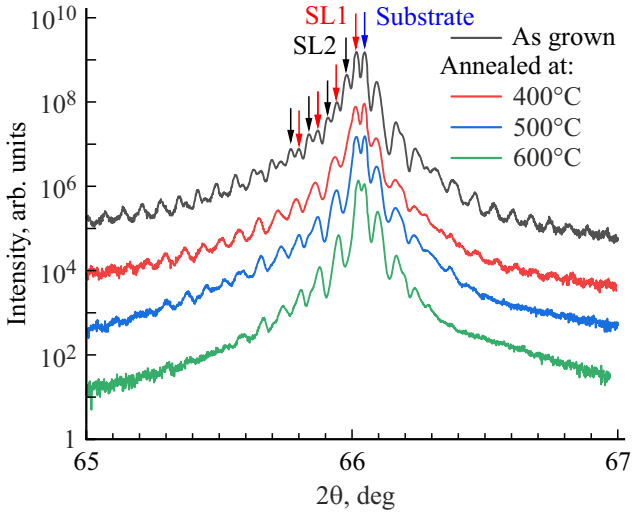

Figure 1. Curves of X-ray diffraction reflection from studied sample before and after annealing at different temperatures. The curves are shifted along the vertical axis for clarity. Blue arrow shows position of diffraction peak 004 of substrate. Red and black arrows indicate main and some satellite diffraction maxima of superlattices SL1 and SL2.

3. Experimental findings

3.1. X-ray diffractometry

Figure 1 presents curves of X-ray diffraction reflection from planes (004) obtained before and after annealing of studied sample at different temperatures. Blue arrow shows position of diffraction peak 004 of substrate. In diffraction curves for unannealed sample part we see two sets of diffraction peaks corresponding to two periodic superlattices (SL1 and SL2) with different mean interplanar spacing. The main diffraction maxima SL1 and SL2, and several satellite reflexes are marked in Figure 1 by red and black arrows. Analysis of the diffraction pattern shows that both superlattices have the same period, equal on average to 147 nm. This value approximately corresponds to the distance between the bismuth delta-layers calculated from the epitaxial growth rate of LT-GaAs. At the same time, for both superlattices the period increases by approximately 1.4 nm in each subsequent period. Curve corresponding to the unannealed sample part demonstrates the most clear oscillations and large number of superstructural maxima, which confirms good planarity of interfaces in structure. SL2 differs from SL1 by different value of mean interplanar spacing.

Figure 1 shows that as result of the sample annealing the diffraction patterns changes. Namely, the oscillations that are associated with SL2 superlattice disappear including main diffraction peak. As a result of after-growth annealing the main SL1 diffraction peak shifts by 0.05% to peak of the substrate. After annealings at temperatures 500 and 600°C there is gradual blurring and attenuation of oscillations determined by superlattice SL1. Since the average interplanar distance in SL2 is greater than in SL1, and the periods of both sublattices are the same, we can conclude that SL2 corresponds to the upper part of the structure that was not annealed during the growth process, and SL1 corresponds to the part of the structure that was subjected to intermediate annealing during the epitaxy process [18]. Change of lattice parameter during annealing is due to precipitation of excess arsenic, captured by GaAs under conditions of low-temperature MBE [24]. in case of the sample studied in present paper the relative change in interplanar spacing in superlattice SL2 as a result of annealing was $\frac{\Delta a}{a} = 5.06 \cdot 10^{-4}$. As per data of paper [25], such change of lattice parameter corresponds to concentration of antisite defects $[As_{Ga}] = 4.1 \cdot 10^{19}\,cm^{-3}$, transformed into system of nanoinclusions. This value $[As_{Ga}]$ corresponds to growth temperature of studied layers about 220°C [23], which is in reasonable agreement with the substrate temperature during MBE of our sample.

As after annealing the concentration of antisite defects becomes small, and they have no significant effect on lattice parameters of the GaAs matrix, mean interplanar spacing in superlattice SL1 can be used to determine bismuth concentration. Assuming lattice parameter of virtual compound GaBi equal to 6.3240 Å [26] the mean content of bismuth in superlattice SL1 is $x_{average} = 0.19\%$. Such mean content of bismuth exactly corresponds to 1 ML of GaBi in each period of superlattice.

3.2. Optical spectroscopy

Simultaneous measurement of spectra of optical transmission T and reflection R ensures determination of the absorption spectrum using obvious relationship: Absorption $= 1 - \frac{T}{1-R}$. The obtained spectra of optical absorption before and after sample annealing at different temperatures are provided in Figure 2. Here the absorption spectrum of GaAs substrate is provided for comparison.

We see from Figure 2 that at wavelength corresponding to energies above the band gap of gallium arsenide, the non-reflected light is completely absorbed. By spectral offset of optical absorption edge we can determine the difference of band gaps in GaAs and $GaAs_{1-x}Bi_x$ [27]. We carried out the corresponding measurements using linear interpolation of the spectrum section 850–950 nm. Offset value was $\Delta E = 1.3$ meV. The bismuth concentration in GaAs corresponding to such change of band gap is $x \approx 0.02\%$ [28,29].

In region of lower wavelength in absorption spectrum in Figure 2 we see „tail" of absorption. For pure GaAs this tail is relatively small, this is inherent to direct-band-gap semiconductors at room temperature [30]. In studied sample the absorption tail is significantly stronger and depends on sample heat treatment. Previously we determined [19,25] that optical absorption in spectral range 1.0–1.1 μm in LT-GaAs, that depends on annealing, occurs due to antisite defects of arsenic As_{Ga}, that form nanoinclusions during

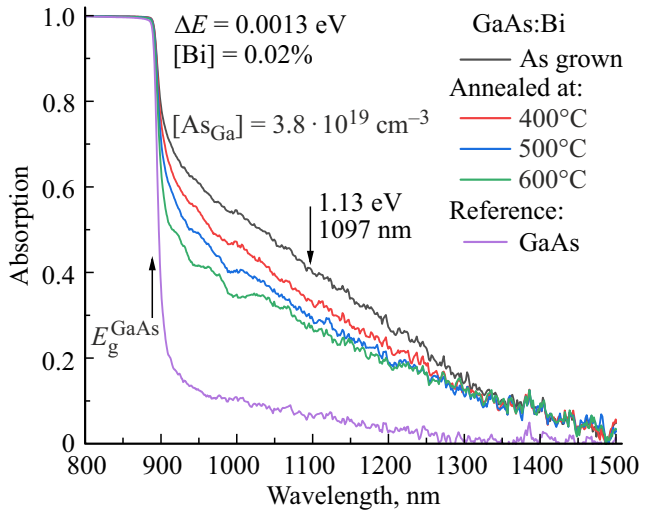

Figure 2. Spectra of optical absorption of sample before and after annealings at different temperatures. Purple curve — absorption spectrum of GaAs substrate. The spectra were measured at temperature of 300 K. Arrow upwards indicates band gap GaAs. Arrow downwards marks wavelength, at which change in absorption spectrum during annealing was measured.

annealing. Knowing change in absorption coefficient of gallium arsenide at wavelength 1000 or 1100 nm, using Martin calibration [31] we can determine concentration of antisite defects. Due to specific nature of the samples growth, all layers of the superlattice, except top five layers, were annealed during MBE. So, in calculations of absorption coefficient determined by antisite defects the thickness of five top layers LT-GaAs was used. To exclude the influence of external absorption processes associated with bismuth, we took the difference in absorption coefficients at wavelength of 1100 nm between the unannealed sample and the sample annealed at 600°C. The obtained difference in coefficients equal to 3049 cm^{-1}, corresponds to concentration of antisite defects $[As_{Ga}] = 3.8 \cdot 10^{19}\ cm^{-3}$.

In Figure 2 attention is drawn to the very significant optical absorption in the region of photon energies below the edge of the fundamental absorption band. This absorption does not disappear after annealings at high temperatures and is associated with the bismuth presence in the structure. The nature of this absorption will not be discussed in this article.

3.3. Transmission electron microscopy

Figure 3 presents dark field image of cross-section of bottom layers of sample, obtained using transmission electron microscopy. Figure field covers region of substrate, two delta-layers of bismuth and three separating layers LT-GaAs. This part of the sample was annealed after growth at 600°C for 15 min. The image shows a well-defined dark contrast formed by quasi-two-dimensional layers of nanoparticles, the position of which coincides with the position of the bismuth delta layers in the gallium arsenide matrix. The characteristic size of nanoparticles in quasi-two-dimensional layers is 10–15 nm.

Besides, in layers of gallium arsenide between delta-layers of bismuth we can see weaker contrast from small precipitations with size of 3–5 nm. Note that the formation of nanoinclusions during annealing is typical phenomenon for LT-GaAs. Reason of this process is large non-equilibrium concentration of antisite defects and vacancies in cation sublattice LT-GaAs. From Figure 3 we see that in region of stoichiometric buffer layer GaAs shown in Figure as GaAs Substrate, no contrast associated with nanoinclusions is observed.

To determine spatial distribution of bismuth in the sample we performed a study by method of X-ray dispersive microanalysis (EDXS), results are presented in Figure 4. In left panel a map of distribution of bismuth concentration

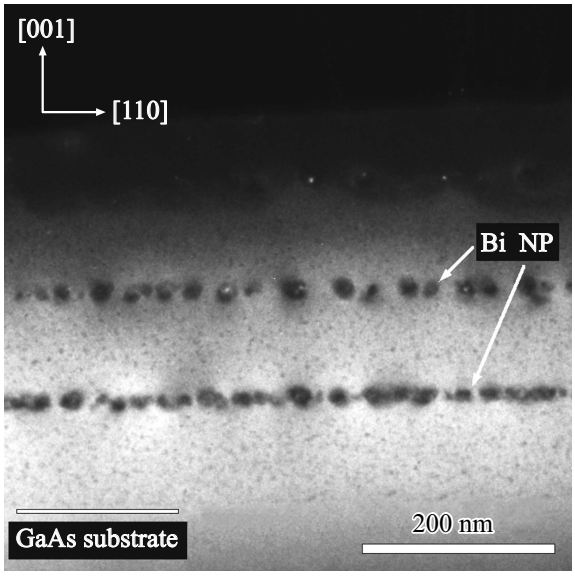

Figure 3. Dark field TEM-image of sample in cross-section (110) in acting reflex 002.

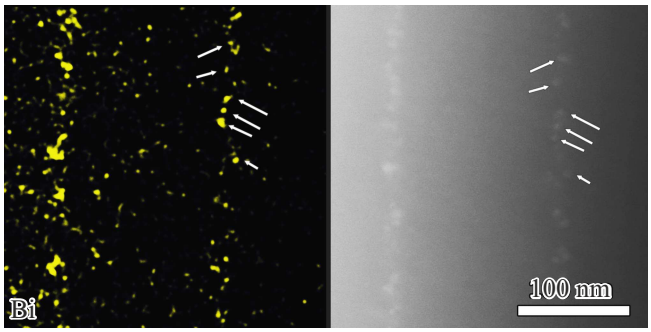

Figure 4. Bismuth distribution map obtained by X-ray dispersive microanalysis (left panel) and the corresponding dark-field image obtained in scanning transmission electron microscopy mode (right panel). Arrows indicate several nanoinclusions of bismuth in quasi-two-dimensional layer.

in relative units is shown in yellow. In right panel a dark-field image of same section of sample obtained in mode of scanning transmission electron microscopy (STEM) is presented. In spite of rather significant noise level, from Figure 4 we see that bismuth distribution is inhomogeneous through the cross-section of the sample. The observed signal associate with bismuth is significantly higher in the region of Bi delta-layers, their projection passes in Figure vertically. At that comparison of images in right and left panels of Figure 4 shows that bismuth is accumulated in nanoinclusions. Such bismuth nanoinclusions are marked in both panels in Figure 4 by arrows.

4. Discussion

Data comparison of X-ray diffraction, optical and electron microscopic studies ensures general picture of the processes occurred during epitaxy and further annealing of sample LT-GaAs with the integral system of bismuth delta-layers.

During low-temperature MBE in LT-GaAs layers non-equilibrium excess of arsenic is formed, mainly in form of antisite defects As_{Ga}. Based on the change of X-ray diffraction pattern after annealing we can conclude that the concentration of antisite defects in unannealed LT-GaAs is $[As_{Ga}] = 4.1 \cdot 10^{19}\,cm^{-3}$. Concentration of such antisite defects can be independently determined from the change in optical absorption at calibrated wavelength 1100 nm. By this method the concentration value was obtained: $[As_{Ga}] = 3.8 \cdot 10^{19}\,cm^{-3}$. The values obtained by two independent methods are in a good agreement. Structural transformations that cause decrease in the concentration of antisite defects are leading to the formation of arsenic nanoinclusions in GaAs matrix [19,20,24,25]. Presence of such nanoinclusions is confirmed by TEM patterns.

Spectra of optical absorption show that edge of band of interband transitions corresponding to the band gap of LT-GaAs is slightly shifted to the region of lower energies. Such offset can be associated with presence of some portion of bismuth in the layer of gallium arsenide that can ingress during growth or annealing. The experiments show decrease in the band gap equal to 1.3 meV, this corresponds to bismuth concentration $x \approx 0.02\%$ in solid solution of $GaAs_{1-x}Bi_x$. So, bismuth segregation under conditions of low-temperature MBE, and bismuth diffusion during intermediate and after-growth annealings do not result in any significant mixing of grown superlattice of bismuth delta-layers. This conclusion is confirmed by the analysis of the superlattice diffraction pattern in X-ray DRC, as well as by EDXS pattern.

The electron microscopic studies documented formation of the quasi-two-dimensional layers of nanoparticles enriched by bismuth, their spatial arrangement coincides with position of bismuth delta-layers formed during epitaxy. Size of nanoinclusions in the quasi-two-dimensional layer is 10−15 nm. These quasi-two-dimensional layers of bismuth nanoparticles are separated by layers of LT-GaAs with low Bi content, in which, in turn, system of small (3−5 nm) nanoinclusions is formed.

5. Conclusion

In present paper we for the first time receive quasi-two-dimensional layers of bismuth nanoparticles in matrix of epitaxial gallium arsenide. We show that the formation of such layers of nanoparticles can be implemented by delta-doping of gallium arsenide layers with bismuth during low-temperature MBE with further annealing. We identified that low-temperature epitaxy ensures formation in bulk of the material of high concentration of defects of non-stoichiometry, first of all antisite defects $[As_{Ga}]$ and gallium vacancies. These defects migration during annealing leads in the formation of both fine precipitations in LT-GaAs layers, and more coarse nanoinclusions enriched with bismuth and located on Bi delta-layers.

Funding

This study was supported by grant of the Russian Science Foundation and St. Petersburg Science Foundation No. 24-22-20012, https://rscf.ru/project/24-22-20012/.

Conflict of interest

The authors declare that they have no conflict of interest.

References

[1] S.A. Maier. Plasmonics: Fundamentals and Applications. Springer, N.Y. (2007).
[2] L. Wang, M. Hasanzadeh Kafshgari, M. Meunier. Adv. Funct. Mater. **30**, *51*, 2005400 (2020).
[3] N. Rivera, I. Kaminer. Nature Rev. Phys. **2**, *10*, 538 (2020).
[4] A.N. Koya, M. Romanelli, J. Kuttruff, N. Henriksson, A. Stefancu, G. Grinblat, A. De Andres, F. Schnur, M. Vanzan, M. Marsili, M. Rahaman, A. Viejo Rodríguez, T. Tapani, H. Lin, B.D. Dana, J. Lin, G. Barbillon, R.P. Zaccaria, D. Brida, D. Jariwala, L. Veisz, E. Cortés, S. Corni, D. Garoli, N. Maccaferri. Appl. Phys. Rev. **10**, *2*, 021318 (2023).
[5] V.E. Babicheva. Nanomaterials **13**, *7*, 1270 (2023).
[6] B.P. Nanda, P. Rani, P. Paul, R. Bhatia. J. Pharmaceutical Analysis (2024). In press. https://doi.org/10.1016/j.jpha.2024.02.013
[7] A.J. Haes, L. Chang, W.L. Klein, R.P. Van Duyne. J. Am. Chem. Soc. **127**, *7*, 2264 (2005).
[8] P. Mandal. Plasmonics **17**, *3*, 1247 (2022).
[9] I.I. Zamkoye, B. Lucas, S. Vedraine. Nanomaterials **13**, *15*, 2209 (2023).
[10] L. Agiotis, M. Meunier. Laser Photon. Rev. **16**, *10*, 2200076 (2022).
[11] R. Rajamanikandan, K. Sasikumar, S. Kosame, H. Ju. Nanomaterials **13**, *2*, 290 (2023).
[12] C. Zhang, C. Huang, M. Pu, J. Song, Z. Zhao, X. Wu, X. Luo. Sci. Rep. **7**, *1*, 5652 (2017).
[13] M. Fleischmann, P.J. Hendra, A.J. McQuillan. Chem. Phys. Lett. **26**, *2*, 163 (1974).

[14] S. Bai, X.L. Ren, K. Obata, Y. Ito, K. Sugioka. Opto-Electron. Adv. **5**, *10*, 210121 (2022).
[15] Y. Wang, X. Xu, Y. Li, C. Li, X. Wang, J. Wu, Y. Li. Talanta **269**, 125432 (2024).
[16] N.A. Toropov, I.A. Gladskikh, P.V. Gladskikh, A.N. Kosarev, V.V. Preobrazhenskiĭ, M.A. Putyato, B.R. Semyagin, V.V. Chaldyshev, T.A. Vartanyan. J. Opt. Technol. **84**, *7*, 459 (2017).
[17] V.I. Ushanov, S.V. Eremeev, V.M. Silkin, V.V. Chaldyshev. Nanomaterials **14**, *1*, 109 (2024).
[18] V.I. Ushanov, V.V. Chaldyshev, V.V. Preobrazhenskii, M.A. Putyato, B.R. Semyagin. Semiconductors **50**, *12*, 1595 (2016).
[19] L.G. Lavrent'eva, M.D. Vilisova, V.V. Preobrazhenskii, V.V. Chaldyshev. Crystallogr. Rep. **47**, *1*, S118 (2002).
[20] V.V. Chaldyshev. Mater. Sci. Eng. B **88**, *2–3*, 195 (2002).
[21] M. Wu, E. Luna, J. Puustinen, M. Guina, A. Trampert. Nanotechnol. **25**, *20*, 205605 (2014).
[22] N. Baladés, D.L. Sales, M. Herrera, C.H. Tan, Y. Liu, R.D. Richards, S.I. Molina. Nanoscale Res. Lett. **13**, 125 (2018).
[23] R. Butkutė, G. Niaura, E. Pozingytė, B. Čechavičius, A. Selskis, M. Skapas, V. Karpus, A. Krotkus. Nanoscale Res. Lett. **12**, 436 (2017).
[24] N.A. Bert, A.I. Weinger, M.D. Vilisova, S.I. Goloshchapov, I.V. Ivonin, S.V. Kozyrev, A.E. Kunitsyn, L .G. Lavrentieva, D.I. Lubyshev, V.V. Preobrazhensky, B.R. Semyagin, V.V. Tretyakov, V.V. Chaldyshev, M.P. Yakubenya. FTT **35**, *10*, 2609 (1993). (in Russian)
[25] X. Liu, A. Prasad, J. Nishio, E.R. Weber, Z. Liliental-Weber, W. Walukiewicz. Appl. Phys. Lett. **67**, *2*, 279 (1995).
[26] A. Janotti, S.H. Wei, S.B. Zhang. Phys. Rev. B **65**, *11*, 115203 (2002).
[27] B.R. Semyagin, A.V. Kolesnikov, M.A. Putyato, V.V. Preobrazhenskii, T.B. Popova, V.I. Ushanov, V.V. Chaldyshev. Semiconductors **56**, *3*, 201 (2022).
[28] A.R. Mohmad, F. Bastiman, J.S. Ng, S.J. Sweeney, J.P.R. David. Physica Status Solidi C **9**, *2*, 259 (2012).
[29] R. Kudrawiec, J. Kopaczek, M.P. Polak, P. Scharoch, M. Gladysiewicz, J. Misiewicz, R.D. Richards, F. Bastiman, J.P.R. David. J. Appl. Phys. **116**, *23*, 233508 (2014).
[30] J.I. Pankove. Optical Processes in Semiconductors. Dover Pub., N.Y. (1971). ISBN 0-486-60275-3
[31] G.M. Martin. Appl. Phys. Lett. **39**, *9*, 747 (1981).

Translated by I.Mazurov